Interaction of cavitating grain boundary facets in creeping polycrystals

Giessen, E. van der; Tvergaard, V.

Published in:
Mechanics of Materials

DOI:
10.1016/0167-6636(94)90013-2

Publication date:
1994

Mechanics of Materials 17 (1994) 47–69
Elsevier

Interaction of cavitating grain boundary facets in creeping polycrystals

E. van der Giessen

Delft University of Technology, Laboratory for Engineering Mechanics, Delft, The Netherlands

V. Tvergaard

The Technical University of Denmark, Department of Solid Mechanics, Lyngby, Denmark

Received 20 March 1992; revised version received 30 October 1992

A plane strain unit cell model containing a periodic array of hexagonal grains is used to analyse creep fracture in polycrystalline metals at elevated temperatures, taking into account the effect of sliding at all grain boundaries. The grains deform elastically and by power law creep, and the possibility of cavity nucleation and growth at the grain boundaries is incorporated. For a single cavitating grain boundary facet, or a single facet microcrack, the effect of microcrack density or spacings is studied by varying the number of grains in the unit cell or the aspect ratio of the unit cell. In cases where creep constrained cavitation develops, and for open microcracks, a significant effect of crack density and cell aspect ratio is found. The multi-grain unit cells are also used to study the influence of nonuniform distributions of cavitating facets such as facet clustering, where strong interaction between neighbouring cavitating facets tends to develop.

1. Introduction

In polycrystalline metals subject to creep at elevated temperatures, failure is often associated with intergranular cavitation and intergranular microcracking. Cavities tend to nucleate and grow most rapidly at grain boundary facets normal to the maximum principal stress direction, and coalescence of such cavities leads to the formation of facet microcracks (Cocks and Ashby, 1982; Argon, 1982). Final intergranular failure occurs as these microcracks link up.

A number of micromechanical studies of creep failure have focussed on the time to cavity coalescence on a characteristic grain boundary facet, and this time has been used as an estimate of the life time. Either a single cavitating facet or a periodic array of cavitating facets have been considered (Rice, 1982; Tvergaard, 1984), and some studies have also incorporated the effect of grain boundary sliding on the rate of nucleation and growth of grain boundary cavities (Anderson and Rice, 1985; Tvergaard, 1985; Van der Giessen and Tvergaard, 1991a). Axisymmetric model problems have been considered in most of these analyses, to obtain a reasonably realistic approximation of the real three-dimensional facet geometry, but still avoiding a full 3D analysis.

The interaction between neighbouring cavitating facets is accounted for in the axisymmetric cell model analyses, but the final process of linking-up of facet microcracks is not well represented by these models. A planar model of a polycrystal gives a less accurate description of real facet geometries; but this type of model can be used to obtain some insight in the linking-up process, as has been done by Van der Giessen and Tvergaard (1991b) for a unit cell covering two neighbouring grains. A larger plane strain unit cell covering several hexagonal grains in each

Correspondence to: Prof. V. Tvergaard, The Technical University of Denmark, Department of Solid Mechanics, Building 404, DK-2800 Lyngby, Denmark.

SSDI 0167-6636(93)E0036-2

coordinate direction has been used by Hsia et al. (1991) to study the effect of microcrack density and free grain boundary sliding on the rate of opening of a facet microcrack.

In the present paper a larger plane strain unit cell containing many hexagonal grains is used to study the interaction between different cavitating facets. Grain boundary sliding as well as the possibility of cavity nucleation and growth is accounted for on all grain boundary facets, but some facets are assumed to cavitate much earlier than others. Effects of both distribution and density of such facets subject to early cavitation are studied.

2. Formulation of the problem

2.1. The polycrystal model

The present study is carried out in terms of a 2D model of a polycrystalline material consisting of a planar array of hexagonal grains as shown in Fig. 1. The polycrystal is taken to be subjected to a macroscopic stress state specified by principal true stresses Σ_1 and Σ_2 under plane strain conditions, with Σ_2 being the maximum principal stress. We consider situations were cavitation takes place on a number of grain boundary facets normal to the direction of the maximum principal stress, or where full facet microcracks are present due to previous cavity coalescence. It is assumed that the spatial distribution of cavitated facets possesses a certain periodicity, so that we can identify a unit cell consisting of $(m_1 \times m_2)$ grains with which the entire polycrystal can be built up by translations of the cell along its sides (for the example shown in Fig. 1, $m_1 = 6$, $m_2 = 5$). It is also assumed that the distribution of cavitated facets exhibits reflective symmetries with respect to its four sides, so that attention can be confined to the quadrant of the cell shown by the hatched region in Fig. 1. This quarter unit cell to be analyzed is shown in more detail in Fig. 2. Due to the symmetries, the

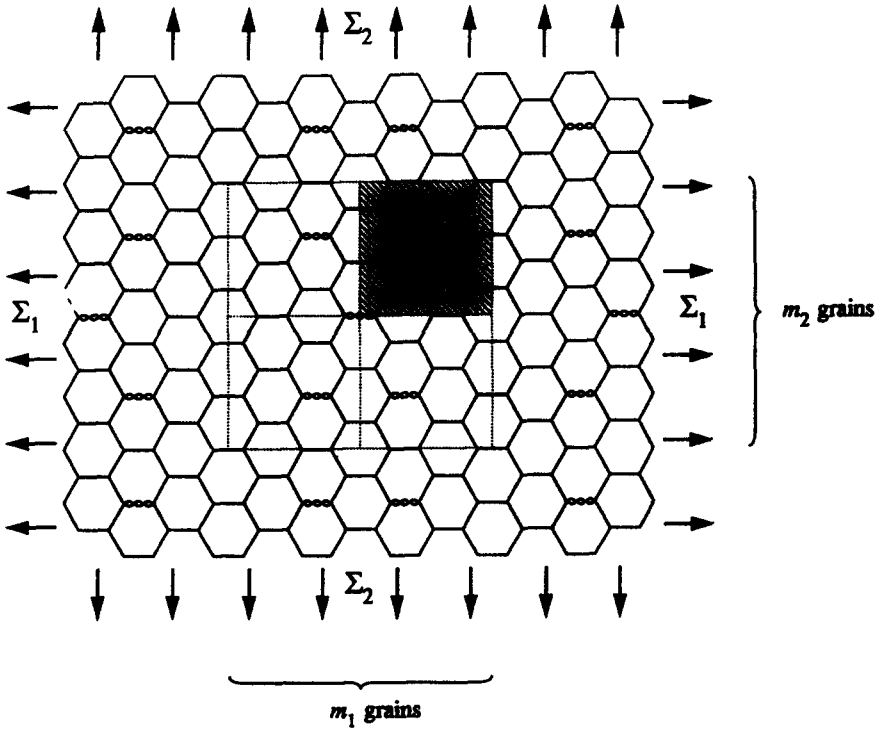

Fig. 1. Two-dimensional polycrystal model. The dashed rectangle is the periodic unit cell consisting of m_1 by m_2 grains. Only the hatched quadrant needs to be analyzed.

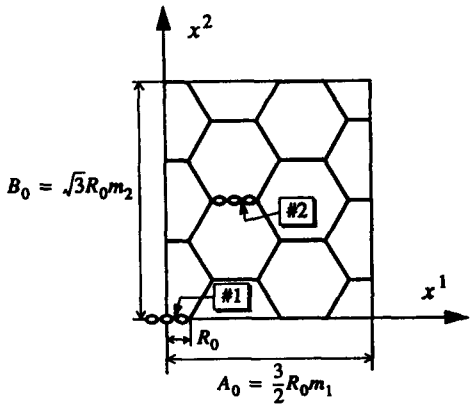

Fig. 2. The quarter cell corresponding to a $(m_1 \times m_2)$ unit cell used in the analysis.

four faces of the quarter unit cell will remain straight and aligned with the coordinate axes x^1 and x^2, and will support no shear stress. The geometry of the unit cell is specified here in terms of the tuple (m_1, m_2) which, together with the initial width $2R_0$ of a grain boundary facet, defines the dimensions A_0, B_0 of the cell. In most of the analyses, the central transverse facet, denoted #1 in Fig. 2 is taken to be cavitating or cracked, and the dimensions of the unit cell control whether or not there is interaction with other cavitating or cracked facets. In some cases the effect of clustering is studied by taking one or more other facets within the unit cell to be cavitating as well, such as facet #2.

Then, if there are M cavitating grain boundary facets in the unit cell, the number of cavitating facets per unit initial area N_f is given by $N = M/(m_1 m_2 A_G)$, where $A_G = 6\sqrt{3}R_0^2$ is the initial undeformed area of a hexagonal grain. With this, the nondimensional cavitating facet density $\rho = N_f R_0^2$ can be obtained in terms of the cell parameters (m_1, m_2) as $\rho = M/(6\sqrt{3}m_1 m_2)$. It is important to note that this density is only a partial characterization of the cavitation state of the polycrystal and does not contain information about the morphology, i.e., the spatial distribution of the cavitating facets. In particular, even if only the central facet #1 is cavitating, the morphology depends on the aspect ratio of the unit cell as specified by m_2/m_1.

The polycrystal model discussed here is an extension of the planar model used previously to investigate the development of microcracks due to cavity coalescence (Van der Giessen and Tvergaard, 1991b,c). Focusing attention on the final stages of the creep rupture process where there is a high density of cavitating facets, the latter model exclusively incorporated a rather small unit cell geometry of $(m_1, m_2) = (2, 1)$, whereas here we will focus mainly on relatively low cavitating facet densities. Also, the present model is akin to the 2D model used by Hsia et al. (1991) to investigate the combined effect of microcracks and grain boundary sliding on the overall creep behaviour of polycrystalline materials. However, grain boundary cavitation was not taken into account in their study and only a single microcrack at the central transverse grain boundary facet was considered.

As pointed out by Anderson and Rice (1985), the deformation of grains in a real 3D polycrystal is much more constrained by that of their neighbouring grains than in the plane strain model considered here. The transition from 2D results to the 3D case is far from being clear, as also discussed by Hsia et al. (1991), and therefore care should be exercised with the interpretation of 2D studies; this will be discussed later in detail. Anderson and Rice (1985) suggested a model in terms of a 3D array of grains represented by so-called Wigner–Seitz cells. This model is applicable to the situation where all facets normal to the maximum principal stress are (equally) cavitated, but such a situation is not representative for the major part of the lifetime. It is not clear yet if and how their approach can be extended to cases with a lower density of cavitating facets. In order to capture some of the 3D constraint effect, Tvergaard (1984, 1985) and subsequently Van der Giessen and Tvergaard (1991a) considered an axisymmetric model. Figure 3 shows how such an axisymmetric model, along with its plane strain counterpart, can be constructed starting out from the periodic array shown in Fig. 1 with a (2, 1) unit cell. In the plane strain model, the grains are box-shaped with a hexagonal cross-section and unit thickness; the parameter N_f introduced above can then be identified equivalently by the number

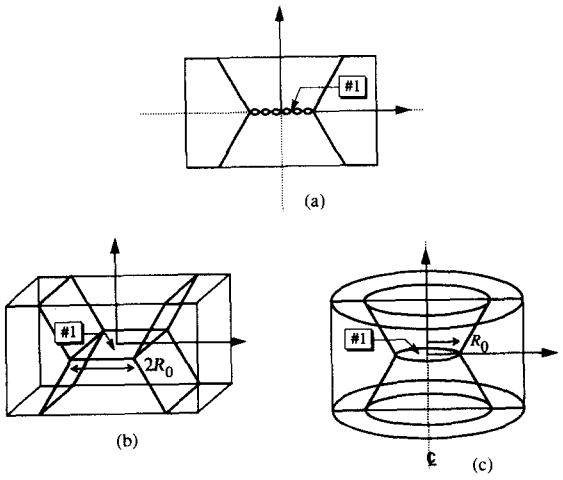

Fig. 3. (a) Grain arrangements for a unit cell of $(m_1, m_2) = (2, 1)$; (b) 3-D interpretation of the planar model; and (c) of the axisymmetric model.

of cavitating facets per unit volume. In this axisymmetric model, the central facet #1 is a disk with radius R_0 and each of the two adjacent central grains are represented by truncated cones; the surrounding grains are represented by a ring of material having a cross-section of a half hexagonal. The density of cavitating facets for the axisymmetric model may be specified by $\rho_A = N_A R_0^3$ where N_A is the number of cavitating facets per unit volume. Some of the computations to be reported on here are carried out for the plane strain as well as the axisymmetric model, and the differences will be discussed.

2.2. Governing equations

The material inside the grains is taken to deform by power-law creep. In addition, grain boundary sliding is accounted for, and also failure by the nucleation and growth of grain boundary cavities to coalescence is incorporated in the model.

Finite strains are accounted for in the analyses, using a convected coordinate formulation of the governing equations. The covariant components of the Lagrangian strain tensor are denoted by η_{ij}, with indices ranging from 1 to 3, and the contravariant components τ^{ij} of the Kirchhoff stress tensor on the current base vectors are defined in terms of the Cauchy stress tensor σ^{ij} by

$$\tau^{ij} = \sqrt{G/g}\,\sigma^{ij}.$$

Here, G and g are the determinants of the metric tensors G_{ij} and g_{ij} in the current configuration and in the reference configuration, respectively.

The total strain-rate $\dot{\eta}_{ij}$ is taken to be the sum of the elastic part $\dot{\eta}^{E}_{ij}$ and the creep part $\dot{\eta}^{C}_{ij}$. Thus, with the elastic stress–strain relationship $\overset{\nabla}{\tau}{}^{ij} = R^{ijkl}\dot{\eta}^{E}_{kl}$, in terms of the Jaumann stress-rate $\overset{\nabla}{\tau}{}^{ij} = \dot{\tau}^{ij} + (G^{ik}\tau^{jl} + G^{jk}\tau^{il})\dot{\eta}_{kl}$, the constitutive relations for the elastic–creeping material can be written as

$$\overset{\nabla}{\tau}{}^{ij} = R^{ijkl}\left(\dot{\eta}_{kl} - \dot{\eta}^{C}_{kl}\right).$$

The creep part of the Lagrangian strain-rate, representing power-law creep, is given by

$$\dot{\eta}^{C}_{ij} = \dot{\epsilon}^{C}_{e}\frac{3}{2}\frac{s_{ij}}{\sigma_e}, \quad \dot{\epsilon}^{C}_{e} = \dot{\epsilon}_0\left(\frac{\sigma_e}{\sigma_0}\right)^n, \tag{1}$$

where $\dot{\epsilon}_0$ and σ_0 are reference strain-rate and stress quantities, and n is the creep exponent. The effective Mises stress $\sigma_e = \sqrt{3 s_{ij} s^{ij}/2}$ and the stress deviator $s^{ij} = \tau^{ij} - G^{ij}\tau^{k}_{k}/3$ are here specified directly in terms of the Kirchhoff stresses τ^{ij}, since the relative volume change $\sqrt{G/g} - 1$ is entirely due to elastic strains, which remain small.

The grain boundary cavities grow by diffusion as well as by creep of the surrounding material. For a grain boundary facet normal to the maximum principal tensile stress, such as those shown in Figs. 1 and 2, approximate expressions for the rate of growth have been developed (Sham and Needleman, 1983; Tvergaard, 1984). Thus, if the cavity radius is a, the average spacing is $2b$ and the cavities maintain the quasi-equilibrium spherical-caps shape (see Fig. 4), the volumetric growth rate $\dot{V}$ of a single cavity may be expressed as

$$\dot{V} = \dot{V}_1 + \dot{V}_2, \quad \text{for} \quad a/L \leqslant 10,$$
$$f = \max\left[\left(\frac{a}{b}\right)^2, \left(\frac{a}{a + 1.5L}\right)^2\right], \tag{2}$$

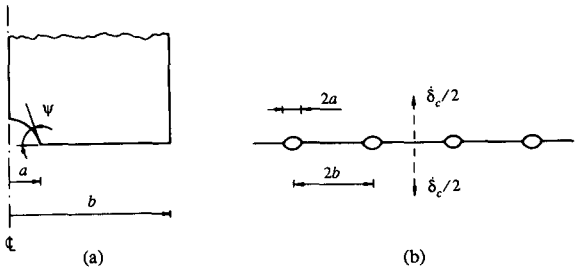

Fig. 4. (a) Geometry of a cavity in the spherical caps shape; (b) equally spaced cavities on a grain boundary.

where

$$\dot{V}_1 = 4\pi\mathscr{D}\frac{\sigma_n - (1-f)\sigma_s}{\ln(1/f) - \frac{1}{2}(3-f)(1-f)}, \tag{3}$$

$$\dot{V}_2 = \begin{cases} \pm 2\pi\dot{\epsilon}_e^C a^3 h(\psi)(\alpha_n|\sigma_m/\sigma_e| + \beta_n)^n, \\ \quad \pm\sigma_m/\sigma_e > 1, \\ 2\pi\dot{\epsilon}_e^C a^3 h(\psi)(\alpha_n + \beta_n)^n \sigma_m/\sigma_e, \\ \quad |\sigma_m/\sigma_e| \leqslant 1. \end{cases} \tag{4}$$

Here, $\mathscr{D} = D_B\delta_B\Omega/kT$ is the grain boundary diffusion parameter, with $D_B\delta_B$ denoting the boundary diffusivity, Ω the atomic volume, k the Boltzmann constant and T the absolute temperature. Furthermore, σ_n is the average stress normal to the current orientation of the grain boundary in the vicinity of the void, and σ_m and σ_e are the average mean and effective stress, respectively. The constants are given by $\alpha_n = 3/2n$, $\beta_n = (n-1)(n+0.4319)/n^2$ and the cavity shape parameter h is defined by

$$h(\psi) = \left[(1+\cos\psi)^{-1} - \tfrac{1}{2}\cos\psi\right]/\sin\psi.$$

The cavity tip angle ψ will be chosen as $\psi = 75°$ and the sintering stress σ_s in (3) will be neglected. The parameter

$$L = \left(\mathscr{D}\sigma_e/\dot{\epsilon}_e^C\right)^{1/3}, \tag{5}$$

in (2) serves as a stress and temperature dependent length scale as discussed by Needleman and Rice (1980). For $a/L < 0.1$ cavity growth is completely dominated by diffusion, whereas for higher values of a/L creep growth plays an increasing role. With $\dot{V}$ according to (2), the growth rate of the cavity radius is found as $\dot{a} = \dot{V}/[4\pi a^2 h(\psi)]$.

Cavities on a grain boundary facet result in an average separation $\delta_c = V/(\pi b^2)$ of the two adjacent grains, where V and b are the current cavity volume and the average half spacing. Thus, the rate of separation is given by

$$\dot{\delta}_c = \frac{\dot{V}}{\pi b^2} - \frac{2V}{\pi b^2}\frac{\dot{b}}{b}. \tag{6}$$

The idea of representing cavities on a grain boundary facet in terms of an average separation δ_c was introduced by Rice (1981) to study creep constrained diffusive cavitation in creeping polycrystals, and was adopted subsequently by Tvergaard (1984, 1985). In his simplified analysis, Rice (1981) made the approximation that all cavities on a single facet were of the same size, and replaced the cavitated facet by a penny-shaped crack with an average opening displacement of δ_c, in order to use a closed form expression for the average rate of opening of such a crack in a creeping material to determine the creep constrained cavity growth rate. Recognizing that the actual facet stress and separation rate will be nonuniform over the facet, Tvergaard (1984, 1985) extended Rice's idea to allow for a continuous variation of σ_n and δ_c along each cavitating facet surface. In the present work, as in Tvergaard (1984, 1985), the creep deformations of the adjacent grains are determined by a numerical solution, as will be discussed in the next section. The variation of δ_c can represent a variation of the cavity volume V as well as of the cavity spacing b along the facet.

Clearly, the representation of grain boundary cavities in terms of a continuous variation of δ_c over a grain boundary facet, presumes that the cavity spacing is significantly smaller than the facet length. This is a reasonable approximation for many metals, as has been shown experimentally by micrographs of polished sections (Hull and Rimmer, 1959; Ashby and Dyson, 1984; Riedel, 1985; Saxena and Bassani, 1984) or by SEM showing fine dimples left by cavities on intergranular fracture surfaces (Chen and Argon, 1981; Dyson and Loveday, 1980).

Experimental observations of cavity nucleation (Dyson, 1983; Argon, 1982) show that the number of cavities grows continuously, mainly as a function of the effective strain. This may be expressed by the evolution equation (Tvergaard, 1985; Van der Giessen and Tvergaard, 1990)

$$\dot{N} = F_n(\sigma_n/\Sigma_0)^2 \dot{\epsilon}_e^C, \tag{7}$$

where N is the number of cavities per unit undeformed grain boundary area, and F_n and Σ_0 are material constants. The effect of nucleation is expressed in terms of the corresponding reduction of the average cavity spacing

$$\frac{\dot{b}}{b} = \frac{1}{2}\dot{\epsilon}_I - \frac{1}{2}\frac{\dot{N}}{N}, \tag{8}$$

to be substituted into (6). Here, $\dot{\epsilon}_I$ is the principal logarithmic strain-rate in the grain boundary plane. As emphasized by Tvergaard (1985), the expressions (7) and (8) for the effect of nucleation imply the significant simplification that at a given point of the facet, newly nucleated voids are taken to have the same size as older voids. In principle, the growth of cavities nucleated at different times should be followed separately; but small voids grow much faster than larger voids, due to diffusion, and numerical analyses have indicated that smaller voids catch up so rapidly that neglecting the size difference may be a good approximation.

Grain boundary sliding is also incorporated in the present analyses. Based on microscopic, atomistic considerations Ashby (1972) has shown that sliding may be represented by a linear viscous relationship between the shear stress τ in the boundary and the relative sliding velocity $\dot{u}$,

$$\tau = \eta_B \dot{u}/w, \tag{9}$$

where w is the thickness of the boundary. He also gives an explicit expression for η_B for an idealized regular boundary, while Raj and Ashby (1971) give corrections on the value of η_B to account for the influence of various irregularities in the grain boundary. For the purpose of relating the contribution of grain boundary sliding to power-law creep, we introduce the strain-rate like parameter $\dot{\epsilon}_B$ (cf., Ghahremani, 1980; Van der Giessen and Tvergaard, 1991a),

$$\dot{\epsilon}_B = \dot{\epsilon}_0 \Big/ \left(2\sqrt{3}\,\frac{R_0}{w}\eta_B \frac{\dot{\epsilon}_0}{\sigma_0}\right)^{n/(n-1)}. \tag{10}$$

The free sliding limit is characterized by $\dot{\epsilon}_e^C/\dot{\epsilon}_B = 0$, while $\dot{\epsilon}_e^C/\dot{\epsilon}_B \to \infty$ in the limit of no sliding. Free sliding will be assumed in most of the present analyses, but a few studies are carried out with so high grain boundary viscosity that sliding is suppressed.

When the grain boundaries slide freely, the strain-rate field inside a single grain is strongly nonuniform, and the overall creep strain-rate of the polycrystalline aggregate is significantly increased by sliding. Then, assuming that the response of the aggregate remains isotropic, the overall creep strain-rates can still be written on the form (1), but with the effective creep strain rate $\dot{\epsilon}_e^C$ replaced by the modified expression (Crossman and Ashby, 1975)

$$\left(\dot{\epsilon}_e^C\right)^* = \dot{\epsilon}_0 (f^* \sigma_e/\sigma_0)^n, \tag{11}$$

where f^* is a stress enhancement factor ($f^* > 1$).

The relations (2)–(8) are also used for cavity growth on inclined, sliding grain boundaries, even though diffusional growth accompanied by grain boundary sliding may give rise to nonequilibrium void shapes. As discussed by Van der Giessen and Tvergaard (1991a) this approximation is considered reasonable for relatively low sliding rates.

3. Method of analysis

The governing equations for the creeping grains are formulated as in previous work (Van der Giessen and Tvergaard, 1991a) within a linear incremental framework based on an incremental version of the virtual work equation. An equilibrium correction is applied in order to prevent drifting of the solution from the true equilibrium path. A forward gradient approach proposed by Pierce et al. (1984) was used to increase the stable step size, as discussed in detail by Tvergaard (1984).

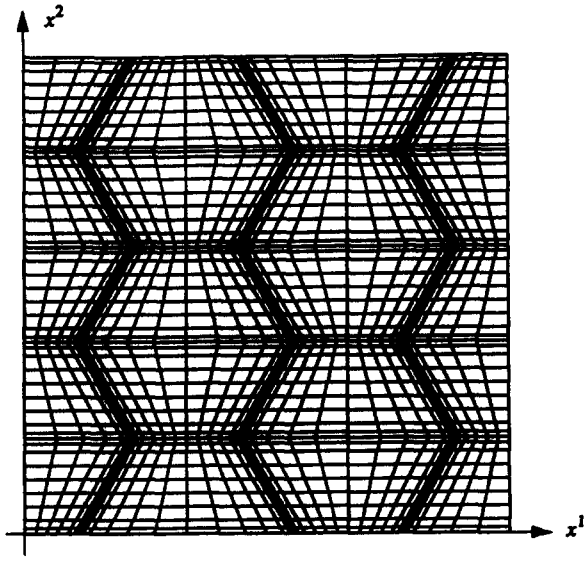

Fig. 5. Finite element mesh used in the numerical analyses of the (6, 5) unit cell. Each quadrilateral is composed of four triangular subelements.

The finite element model of each of the grains uses quadrilateral elements, each built up of four linear displacement triangular subelements arranged in a "crossed triangle" configuration. In the present study, the mesh within each hexagonal grain consists of 12×18 quadrilateral elements. An example of the total mesh for a quarter unit cell is shown in Fig. 5 for the (6, 5) unit cell. The relatively crude mesh used here will not be able to pick-up the strong peaks in the stress fields, etc., near triple points. However, it was found previously in a study with a small unit cell (Van der Giessen and Tvergaard, 1991b) that the cavitation process was only slightly sensitive to the element size; using a finer mesh with twice the number of elements per grain was found to reduce the time to develop a full facet microcrack by only 2% for a typical case.

The cavitation on the sliding grain boundary facets in the polycrystalline aggregate is treated by employing a "smeared out" model. Assuming that the cavities remain small compared to the size of a grain facet, each facet containing a discrete distribution of cavities of radius a and half spacing b, is replaced in the analysis by a grain boundary layer to which continuous distributions $a(x)$ and $b(x)$ are attributed. This procedure is illustrated in Fig. 6. The average separation δ_c between the two adjacent grains due to cavitation, as governed by the evolution law (6) defines the thickness of this grain boundary layer.

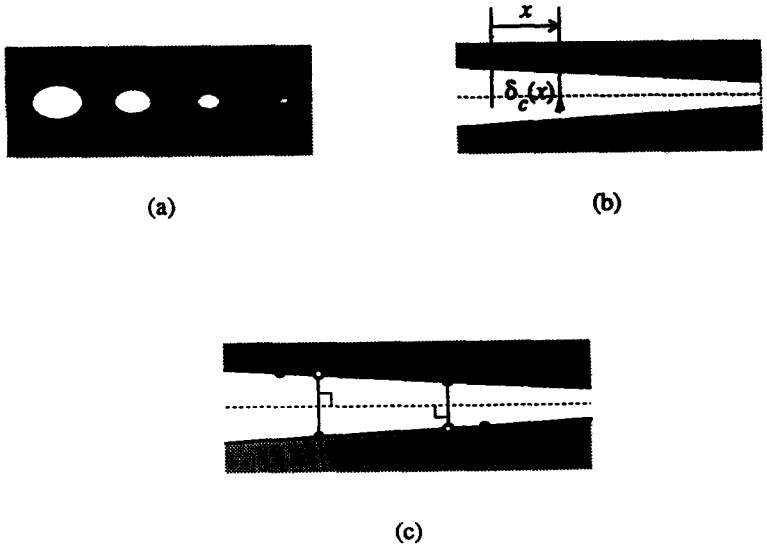

Fig. 6. Illustration of the procedure used to numerically handle cavitating grain boundary facets: (a) individual cavities with varying radius on a grain boundary; (b) 'smeared out' model in terms of a layer of thickness δ_c; (c) discretization of grain boundary layer in terms of grain boundary elements.

Usually, cavitation is not uniform on a grain boundary, and the thickness of the grain boundary layer varies continuously along the facet, $\delta_c = \delta_c(x)$.

In the numerical analysis, special purpose finite elements are used to model the grain boundary layers along the cavitating facets. Details of the procedure used to define these elements at each incremental step as well as the formulation of the governing equations have been given by Van der Giessen and Tvergaard (1991a) for the axisymmetric cell model problem; these considerations immediately carry over to the present plane strain study and will not be repeated here. The grain boundary elements are designed to keep track of the cavitation process, and to account for the associated thickening of the grain boundary layer, according to (6), as well as the viscous grain boundary sliding, according to (9). For computational reasons, two fictitious layers of linear elastic springs are added to the grain boundary layer: one with a stiffness k_n normal to the layer and one with a stiffness k_s tangential to the layer. The normal stress σ_n at the grain boundary and the shear stress τ are then governed by the following constitutive equations

$$\dot{\sigma}_n = k_n\left(\dot{\delta} - \dot{\delta}_c\right), \tag{12}$$

$$\dot{\tau} = k_s\left(\dot{v} - \dot{v}_v\right), \tag{13}$$

with $\dot{\delta}$ and $\dot{v}$ being the actual normal thickening rate and relative sliding velocity, respectively, and with the inelastic components $\dot{\delta}_c$ and $\dot{v}_v$ being given by (6) and by $\dot{v}_v = \tau(\eta_B/w)$ according to (9), respectively. The deviations $\dot{\delta} - \dot{\delta}_c$ and $\dot{v} - \dot{v}_v$ introduced by using these fictitious spring layers is kept very small by using large values of the stiffnesses: $k_n = k_s \approx 10E/R_0$. It should be noted that the grain boundary thickness w appearing in the grain boundary sliding relations (9) and (10) is not to be identified with the thickness δ_c of the grain boundary layer, which is merely a computational entity representing the local average separation between grains due to cavitation. The precise value of w itself need not be specified in this approach; it suffices to specify only the ratio η_B/w in (9), and this can be done conveniently through the parameter $\dot{\epsilon}_B$ defined in (10). Further, it is noted that knowing the precise value of w is not important in cases where $\dot{\epsilon}_B$ is either so large that there is free sliding or so small that sliding is essentially suppressed (as considered in the present paper).

To improve the numerical stability, a forward gradient scheme is used for the integration of the constitutive equations (12) and (13), just as in the integration of the creep constitutive equations. The derivation pertaining to the equations (12) in the normal direction has been given by Van der Giessen and Tvergaard (1991a), and that for the slip relationship (13) follows in a completely similar manner.

For grain boundary facets that coincide with one of the boundaries of the unit cell, a slightly special approach is required. Since the cell boundaries are planes of symmetry, we in fact consider only half grain boundary layers in such cases. The grain boundary elements used are modified to properly account for these symmetries.

The boundary conditions applied to one quadrant of the unit cell (see Fig. 2) read

$$\begin{aligned}
&\dot{u}^1 = 0, \quad T^2 = 0, \quad \text{along} \quad x^1 = 0;\\
&\dot{u}^1 = \dot{U}_I, \quad T^2 = 0, \quad \text{along} \quad x^1 = A_0;\\
&\dot{u}^2 = 0, \quad T^1 = 0, \quad \text{along} \quad x^2 = 0;\\
&\dot{u}^2 = \dot{U}_{II}, \quad T^1 = 0, \quad \text{along} \quad x^2 = B_0;
\end{aligned}$$

in terms of the velocity components $\dot{u}^i$ and the nominal tractions T^i in the reference configuration. The uniform velocities $\dot{U}_I$ and $\dot{U}_{II}$ are determined by means of a special Rayleigh–Ritz technique (Needleman and Tvergaard, 1984) so that the average stresses Σ_1 and Σ_2, respectively, as computed from

$$\Sigma_1 = \frac{1}{B}\int_0^{B_0} T^1\Big|_{x^1=A_0}\,\mathrm{d}x^2,$$

$$\Sigma_2 = \frac{1}{A}\int_0^{A_0} T^2\Big|_{x^2=B_0}\,\mathrm{d}x^1,$$

respectively, retain specified constant values. Here, $A = A_0 + U_I$ and $B = B_0 + U_{II}$ are the di-

mensions of the cell in the current deformed state.

4. Results

In this section we present results of the numerical analyses for a number of different cell geometries and initial conditions. First we consider cases where only the central grain boundary facets, indicated by #1 in Fig. 2, contain a microcrack. We study the effect of microcrack density on the subsequent rate of opening-up of the microcrack, extending the analyses carried out by Hsia et al. (1991). Next, in Section 4.2, we consider situations where cavitation takes place on the #1 facets and study the interaction between such cavitating facets. Finally, in Section 4.3, we investigate the effect of clustering of cavitating facets.

For future reference, we note that the macroscopic effective stress Σ_e corresponding to the applied macroscopic stress Σ_1 and Σ_2 can be approximated by the expression $\Sigma_e = \frac{1}{2}\sqrt{3}\,|\,\Sigma_1 - \Sigma_2\,|$ for pure plane strain creep, while the macroscopic mean stress is approximated by $\Sigma_m = (\Sigma_1 + \Sigma_2)/2$. The grain boundary viscosity is specified in terms of the parameter $\dot{\epsilon}_B$ defined in (10) relative to the macroscopic effective creep rate $\dot{\epsilon}_e^C$ corresponding to the macroscopic effective stress Σ_e according to (1). Completely free grain boundary sliding is characterized by $\dot{\epsilon}_e^C/\dot{\epsilon}_B = 0$, while a very high value of the viscosity specified through $\log(\dot{\epsilon}_e^C/\dot{\epsilon}_B) = 3.5$ was shown by Van der Giessen and Tvergaard (1991a) to simulate the no-sliding condition very well.

4.1. Crack opening rates

The effect of grain boundary sliding and the effect of microcrack density on the rate of crack opening will be discussed here in relation to expressions that have been used to model grain boundary cavitation. For a material subject to grain boundary cavitation, Rice (1981) has suggested modelling the cavitating facets as penny-shaped cracks. Using an expression obtained by He and Hutchinson (1981), modified to account for a non-zero normal tensile stress σ_n on the crack surfaces (Tvergaard, 1984), the average rate of crack opening is given as

$$\dot{\delta}_A = \beta_A^* \frac{S_A^* - \sigma_n}{\sigma_e} \dot{\epsilon}_e^C 2R. \tag{14}$$

Here, R is the current crack radius, β_A is a constant, S_A^* is the value that the normal stress on the facet would have if there was no cavitation, $\dot{\epsilon}_e^C$ is the effective creep strain rate, and it is assumed that the crack is normal to the maximum principal tensile stress. The macroscopic principal true stresses are denoted S and T in the axial and transverse directions, respectively. In the absence of grain boundary sliding the coefficient $\beta_A^* = \beta_A$ of (14) is given by the asymptotic expression (He and Hutchinson, 1981)

$$\beta_A \approx \frac{4}{\pi}\left(1 + \frac{3}{n}\right)^{-1/2}, \tag{15}$$

in terms of the power law creep exponent n. This value (15) is highly accurate for $|\,S/\sigma_e\,| \leqslant 2$, but inaccurate in the high triaxiality range for S/σ_e larger than about 3 or 4.

Based on axisymmetric numerical model studies for freely sliding grain boundaries and well-separated cavitating facets it has been found (Tvergaard, 1985) that with

$$S_A^* = S + c_1^A \tfrac{3}{2}(S - \sigma_m), \quad \beta_A^* = c_2^A \beta_A, \tag{16}$$

and $\sigma_m = (S + 2T)/3$ denoting the mean stress, the average crack opening rate is still reasonably well approximated by (14), if $c_1^A = 1$ and $c_2^A = 4$. If all facets normal to the maximum principal tensile stress are cavitated (Anderson and Rice, 1985) the overall creep rate is strongly increased, and it has been estimated by Tvergaard (1988) that these results are approximately represented by using the values $c_1^A = 1$ and $c_2^A = 200$ in (16).

For the plane strain hexagonal array of grains analysed in the present paper the behaviour is analogous to that described above. He and Hutchinson (1981) have also obtained an expression for the average crack opening rate of a plane strain crack, which may be modified to account

for a non-zero normal tensile stress on the crack surfaces as

$$\dot{\delta} = \beta^* \frac{S^* - \sigma_n}{\sigma_e} \dot{\epsilon}_e^C 2R, \tag{17}$$

similar to (14), and their asymptotic expression for the coefficient $\beta^* = \beta$ in the absence of grain boundary sliding is

$$\beta = \tfrac{3}{8}\pi\sqrt{n}\,.$$

Rice (1981) showed that the expression for S^* follows directly from equilibrium of the system of freely sliding hexagonal grains, and he also suggested using an effective facet radius equal to R plus the projected length of the inclined sliding facet. Thus, we write

$$S^* = S + c_1\left(S - \frac{S+T}{2}\right), \quad \beta^* = c_2\beta, \tag{18}$$

with the value $c_1 = 1$ following directly from equilibrium, and the value $c_2 = 2$ according to Rice (1981). In fact, Rice (1981) used this analysis to obtain an indication of the effect of sliding for a penny shaped crack, results that were used by Tvergaard (1985) to suggest the expression (16).

For an open crack, where $\sigma_n = 0$ in (17) or (14), the distinction between a correction on S^* and a correction on β^*, as in (18) or (16), may seem unnecessary; indeed, this distinction was not made by Hsia et al. (1991). However, in a case where the crack represents a cavitating grain boundary facet (e.g., Rice, 1981; Tvergaard, 1984) the corrected value of the stress S^* plays an important role. The expressions (18) and (16) also include an influence of the transverse stress T, so that both (17) and (14) show a positive crack opening rate for compressive transverse stresses $T < 0$, if $S = 0$. This type of stress triaxiality effect was represented by Hsia et al. (1991) in terms of a functional form that was fitted to numerical results, using a least squares fitting technique.

Now, the present numerical computations, for various sizes and aspect ratios of the unit cell containing a single crack on facets #1 in Fig. 2, can be compared with the predictions of the expression (17) with $S = \Sigma_2$ and $T = \Sigma_1$. In each case the value of the constant c_2 can be calculated so that (17) agrees with the numerical result; but it is emphasized that the requirement $c_1 = 1$ in (18) cannot be adjusted as this value of c_1 is given by equilibrium. Table 1 shows results

Table 1
Computed crack opening rates under uniaxial tension for various cells, various values of n, and with or without grain boundary sliding, as specified through $\dot{\epsilon}_e^C/\dot{\epsilon}_B = 0$ or $\dot{\epsilon}_e^C/\dot{\epsilon}_B \to \infty$, respectively

(m_1, m_2)	ρ	S/Σ_e	T/Σ_e	n	$\dot{\epsilon}_e^C/\dot{\epsilon}_B$	f^*	$\dot{\delta}/\dot{\delta}_{HH}$	c_1	c_2	$\dot{\delta}/(\dot{\delta}_{HH})^*$
(2, 1)	0.0481	1.155	0	5	∞	–	1.72	–	–	1.72
(2, 2)	0.0241	1.155	0	5	∞	–	1.44	–	–	1.44
(2, 4)	0.0120	1.155	0	5	∞	–	1.02	–	–	1.02
(4, 1)	0.0241	1.155	0	5	∞	–	0.82	–	–	0.82
(4, 2)	0.0120	1.155	0	5	∞	–	1.10	–	–	1.10
(6, 3)	0.0053	1.155	0	5	∞	–	1.06	–	–	1.06
(6, 5)	0.0032	1.155	0	5	∞	–	1.13	–	–	1.13
(2, 1)	0.0481	1.155	0	5	0	1.19	30.1	1.0	20.1	12.8
(2, 2)	0.0241	1.155	0	5	0	1.19	29.3	1.0	19.5	12.5
(2, 4)	0.0120	1.155	0	5	0	1.19	10.5	1.0	7.03	4.47
(4, 1)	0.0241	1.155	0	5	0	1.19	4.47	1.0	2.98	1.90
(4, 2)	0.0120	1.155	0	5	0	1.19	8.27	1.0	5.52	3.52
(6, 3)	0.0053	1.155	0	5	0	1.19	6.61	1.0	4.41	2.82
(6, 5)	0.0032	1.155	0	5	0	1.19	7.69	1.0	5.13	3.28
(6, 5)	0.0032	1.155	0	3	0	1.17	4.33	1.0	2.89	2.73
(6, 5)	0.0032	1.155	0	8	0	1.22	20.0	1.0	13.3	4.16

for a number of different cell analyses. Each analysis is characterized by the values of the applied stresses S/Σ_e and T/Σ_e, the power hardening exponent n, the cell size (m_1, m_2), and the corresponding crack density ρ. In each case is given the values of $\dot{\delta}/\dot{\delta}_{HH}$ without sliding and with sliding, respectively, where $\dot{\delta}_{HH}$ is the non-sliding result of He and Hutchinson (1981), and also the value of c_2 corresponding to the free sliding case is given. The $\dot{\delta}$ is the computed average crack opening rate at constant creep rate, while $\dot{\delta}_{HH}$ may be recovered from (17) by substituting $S^* = S$ and $\beta^* = \beta$. In uniaxial plane strain tension ($S > 0$ and $T = 0$) the value $S^* = 1.5S$ is found from (18), and thus $\dot{\delta}/\dot{\delta}_{HH} = 1.5c_2$.

The effective creep strain rate $\dot{\epsilon}_e^C$ appearing in (14) and (17) is that in a homogeneous material without grain boundary sliding, subject to the applied average stress state. Thus, this $\dot{\epsilon}_e^C$ is obtained from the creep law (1) by substitution of the macroscopic effective stress Σ_e. Alternatively, one may wish to normalize the crack opening rate by the overall effective creep strain rate, which is enhanced by grain boundary sliding according to the expression (11) for $(\dot{\epsilon}_e^C)^*$. The value of the He and Hutchinson expression (17) with $c_1 = 0$ and $c_2 = 1$, but with $\dot{\epsilon}_e^C$ replaced by $(\dot{\epsilon}_e^C)^*$, is now denoted $(\dot{\delta}_{HH})^*$, and Table 1 also shows values of $\dot{\delta}/(\dot{\delta}_{HH})^*$. The value of the stress enhancement factor f^* used in (11) for each value of n is obtained from analyses with the polycrystal model assuming no damage at all. The value of f^* is computed from the macroscopic strain-rates during stationary creep, and the values thus obtained agree well with those of Hsia et al. (1991) and Ghahremani (1980).

For no grain boundary sliding, Table 1 shows that the expression (17) is in good agreement with the present cell model analyses ($\dot{\delta}/\dot{\delta}_{HH} \approx 1$), as long as the cells are rather large, corresponding to a small value of the crack density ρ. For larger values of ρ, in the (2, 2) and (2, 1) cells, $\dot{\delta}/\dot{\delta}_{HH} > 1$ indicates that there is increasing interaction between neighbouring cracks, while the high aspect ratio (4, 1) cell shows a shielding effect, so that $\dot{\delta}/\dot{\delta}_{HH} < 1$. The tendencies are most clearly seen by comparing cells with the same aspect ratio, and thus for the (2, 1), (4, 2), and (6, 3) cells the corresponding $\dot{\delta}/\dot{\delta}_{HH}$-values, 1.72, 1.10 and 1.06, respectively, decay systematically towards unity.

With free grain boundary sliding the values of $\dot{\delta}/\dot{\delta}_{HH}$ in Table 1 are much larger than unity, and the corresponding values of c_2 in (17) and (18) are significantly larger than the value 2 suggested by Rice (1981). Also the values of $\dot{\delta}/(\dot{\delta}_{HH})^*$, corresponding to using $(\dot{\epsilon}_e^C)^*$ in (17), are shown, and it is noted that the values around 3 found for the smaller crack densities are in good agreement with results of Hsia et al. (1991). The trends are again seen clearly by comparing the (2, 1), (4, 2), and (6, 3) cells with the same aspect ratio, for which the values of $\dot{\delta}/\dot{\delta}_{HH}$ are 30.1, 8.27 and 6.61, the values of c_2 are 20.1, 5.52 and 4.41, while the values of $\dot{\delta}/(\dot{\delta}_{HH})^*$ are 12.8, 3.52 and 2.82. The indication of these results is that a value of c_2 around 4 should be used in the limit of very small crack densities. The results also show that the crack opening rates not only depend on the crack density ρ, as considered by Hsia et al. (1991), but also on the aspect ratio m_2/m_1 of the periodic pattern. It is noted that precise comparison between the values of $\dot{\delta}/(\dot{\delta}_{HH})^*$ given in Table 1 and the values around 2.7 shown by Hsia et al. (1991) for $\rho = 0.0126$ and $\rho = 0.0071$ has not been possible, because the cell size (m_1, m_2) is not specified by these authors. The mesh plots and stress contour plots shown by Hsia et al. (1991) refer to an (8, 8) cell with $\rho = 0.0015$.

For the largest unit cell considered, the (6, 5) cell, results are also shown for $n = 3$ and $n = 8$. It is seen that the value of c_2 is a strongly increasing function of n. For the same unit cell, Table 2 shows results of different stress states, with the

Table 2
Crack opening rates for the (6, 5) cell ($\rho = 0.0032$) with $n = 5$ for different stress states, normalized by the crack opening rate $\dot{\delta}_u$ in uniaxial tension

(m_1, m_2)	σ_2/σ_e	σ_1/σ_e	$\dot{\delta}/\dot{\delta}_u$	
			numerical	Eq. (17)
(6, 5)	1.155	0.0	1.00	1.00
(6, 5)	0.0	−1.155	0.34	0.33
(6, 5)	1.540	0.385	1.29	1.22
(6, 5)	2.309	1.155	2.02	1.67

value of $\dot{\delta}$ normalized by the value $\dot{\delta}_u$ in uniaxial plane strain tension, since this ratio is independent of c_2 according to (17). It is seen that for transverse compression ($T < 0$ and $S = 0$) the ratio predicted by (17) is in very good agreement with the numerical result. The agreement is also reasonably good for $T/S = 0.25$, but less good for $T/S = 0.5$. Clearly, the main trends in the stress state dependence for free sliding are well represented by (17) for constant c_2, but for high triaxialities the average crack opening rate starts to exceed the value predicted by (17).

For comparison with the plane strain model a few results of axisymmetric or full 3D model studies are shown in Table 3 for uniaxial tension ($S > 0$, $T = 0$). The axisymmetric model (Tvergaard, 1985; Van der Giessen and Tvergaard, 1991a) has a cross-section as that of the (2, 1) cell (see Fig. 3c) and the value of the 3D crack density measure is $\rho_A = 0.0102$, corresponding to reasonably well-separated facet cracks. The full 3D model of an array of freely sliding Wigner–Seitz cells (Anderson and Rice, 1985) has facet cracks at all grain boundary facets normal to the maximum tensile stress, corresponding to $\rho_A \approx 0.04$. For the axisymmetric model, results are shown for no sliding, for free sliding on the conical surface, leading to $f^* = 1.09$, and for an assumed sliding enhancement $f_0^* = 1.09$ in the outer ring of material, leading to $f^* = 1.16$ as discussed by Van der Giessen and Tvergaard (1991a). For these sliding cases the values found for $\dot{\delta}/\dot{\delta}_{HH}$ correspond to $c_2^A = 4.2$ and $c_2^A = 6.5$, whereas the result for the Wigner–Seitz cell gives an exceedingly high c_2^A value of the order of 3000 (based on an approximate expression for $\dot{\delta}$ specified by Anderson and Rice, 1985). The case considered by Anderson and Rice (1985) is the 3D analog of the planar model for $\rho = 0.0962$, where the material falls apart instantaneously. Based on overall strain rates an earlier estimate of c_2^A for the Wigner–Seitz cell was 200; but both values are very large, indicating that when the crack density approaches $\rho_A = 0.04$ the material lifetime is essentially exhausted.

Expressions for full 3D configurations have been suggested by Hsia et al. (1991), based on those determined by their planar cell analyses, by assuming that the relationships between 3D and 2D solutions in the freely sliding case are identical to those found by He and Hutchinson (1981) in the non-sliding case. For overall strain rates, Hsia et al. (1991) find significant disagreement with a 3D expression suggested by Tvergaard (1985) for $c_2^A = 4$ and $c_1^A = 1$; but it appears that they have not noticed that the crack density parameter ρ defined by Hutchinson (1983) is $19\rho_A$ for $n = 5$. However, an important conclusion of the results in Tables 1 and 3 is that in expressions based on equations like (14)–(18) a constant value of c_2 or c_2^A cannot represent all crack densities. In a 2D array the value of c_2 grows very large for $\rho \to 0.096$, and in a 3D array c_2^A grows very large for $\rho \to 0.04$. From the planar cell analyses with several different crack densities (Table 1) it appears that the asymptotic value of c_2 for $\rho \to 0$ should be around 4. In the case of the 3D arrays, the axisymmetric cell models suggest values of c_2^A around 4 to 6, dependent on the sliding enhancement used, but these crack densities are not small enough to guarantee that the asymptotic value of c_2^A, for $\rho_A \to 0$, has been reached.

4.2. Effect of facet interaction on cavitation

In the previous subsection, we have considered various unit cells with a full microcrack at the central grain boundary facet indicated by #1 in

Table 3
Crack opening rates from axisymmetric or full 3D cell model studies, for various grain boundary sliding conditions

Cell type	ρ_A	$\dot{\epsilon}_e^C/\dot{\epsilon}_B$	f_0^*	f^*	$\dot{\delta}/\dot{\delta}_{HH}$	$\dot{\delta}/(\dot{\delta}_{HH})^*$
Fig. 3c	0.0102	∞	–	–	1.06	1.06
Fig. 3c	0.0102	0	1.00	1.09	8.36	5.42
Fig. 3c	0.0102	0	1.09	1.16	12.9	6.15
Wigner–Seitz	~ 0.04	0	–	–	~ 6020	–

Fig. 2. Instead, we here study cavitation processes on that same grain boundary facet, and show the evolution of the damage parameter a/b at the cavitating facet as a function of the normalized time t/t_R. Here, the reference time t_R is defined by $t_R = \Sigma_e/(E\dot{\epsilon}_e^C)$, where E is Young's modulus, and Σ_e and $\dot{\epsilon}_e^C$ are the macroscopic applied effective stress and the corresponding creep rate. All cases to be presented in this subsection are for an applied macroscopic stress state with $\Sigma_e/E = 0.5 \times 10^{-3}$ and $\Sigma_1/\Sigma_2 = 0.5$.

In Fig. 7 we study the cavity growth in a polycrystal with freely sliding grain boundaries, assuming that all cavities on the central facet are present from the beginning. The initial cavitation state is taken to be uniform over the facet and is specified by the initial radius $a_I/R_0 = 0.01$ and by the initial spacing $b_I/R_0 = 0.1$ (note that if the facet would be penny-shaped as in an axisymmetric model, this spacing would correspond to an initial density $N_I = 100/A_I$ with $A_I = \pi R_0^2$). The grain boundary diffusion parameter $\mathscr{D}$ is specified in terms of the length scale L measured relative to the initial cavity radius a_I by the initial value $(a/L)_I = 0.025$. Here, the initial value of L corresponds to substituting the macroscopic effective stress Σ_e into (5). The same unit cells are considered as in the previous section, covering a wide range of the density ρ of cavitating facets (from $\rho = 0.0481$ down to 0.0032) and including various aspect ratios of the unit cell. The smallest (2, 1) unit cell has been studied previously (Van der Giessen and Tvergaard, 1991b,c). Figure 7 shows that cavity growth is influenced rather strongly by the facet density ρ as well as by the aspect ratio m_2/m_1 of the unit cell; but, cavitation remains almost uniform over the facet in all cases. In the early stages of the process up to $t/t_R \approx 0.3$, there is no noticeable effect of interaction, but the final times to cavity coalescence ($a/b \approx 1$) differ up to a factor of about 3. The effect of the cell aspect ratio shows dramatically for the (2, 2) and (4, 1) unit cells which have the same density ρ, but which give rise to the fastest and slowest cavity growth, respectively, among all cases considered here. As noted before, it should be realized that aspect ratios of 1/4 are not very realistic; an aspect ratio m_2/m_1 close to unity, corresponding to a more or less square unit cell, seems to be the most likely one among all possibilities for any given facet density. Taking this into consideration and looking at cells with decreasing value of ρ, it seems reasonable to assume that the results for the (6, 5) cell are close

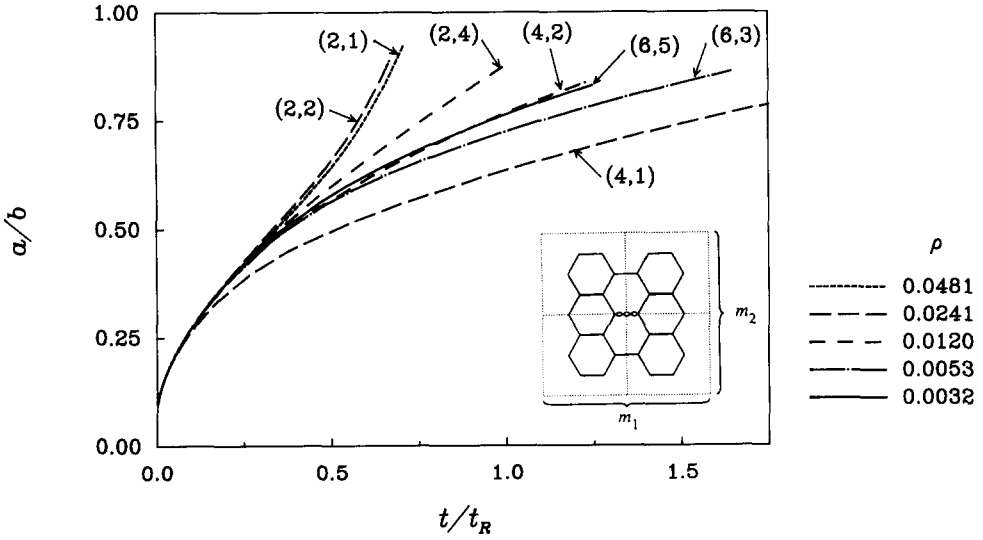

Fig. 7. Development of damage at the center of the central facet #1 in a (m_1, m_2) unit cell with free grain boundary sliding ($\epsilon_e^C/\epsilon_B = 0$) for $\Sigma_1 = 0.5\Sigma_2$, $(a, L)_I = 0.025$ and $F_n = 0$ with $a_I/R_0 = 0.01$ and $b_I/R_0 = 0.1$.

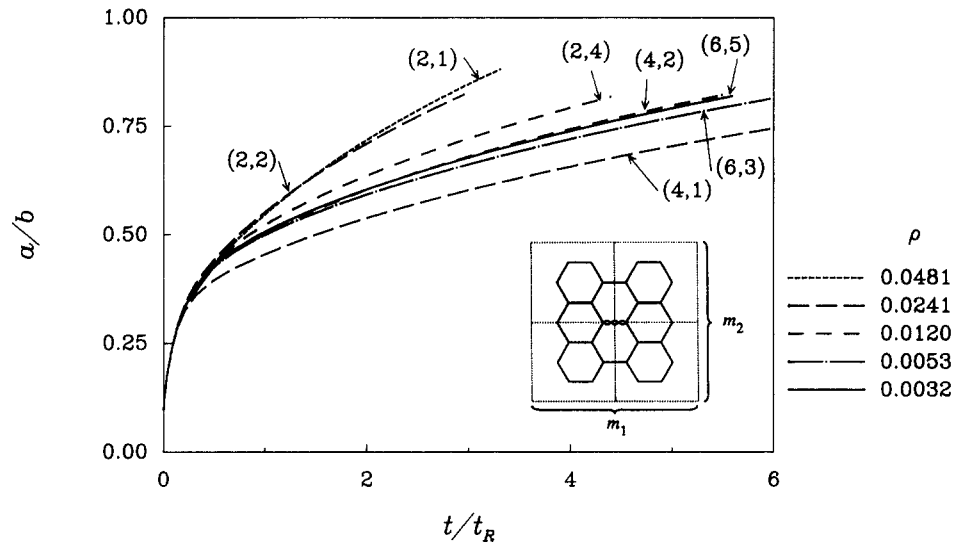

Fig. 8. Development of damage at the center of the central facet #1 in a (m_1, m_2) unit cell with virtually no grain boundary sliding ($\log(\dot{\epsilon}_e^C/\dot{\epsilon}_B) = 3.5$) for $\Sigma_1 = 0.5\Sigma_2$, $(a/L)_I = 0.025$ and $F_n = 0$, with $a_I/R_0 = 0.01$ and $b_I/R_0 = 0.1$.

to representing cavity growth behaviour in cases where cavitating facets are well-separated, so that there is no interaction with neighbouring cavitating facets.

To get some insight into the effect of grain boundary sliding in the above results, the cases of Fig. 7 have been repeated without sliding ($\log(\dot{\epsilon}_e^C/\dot{\epsilon}_B) = 3.5$), but with otherwise identical

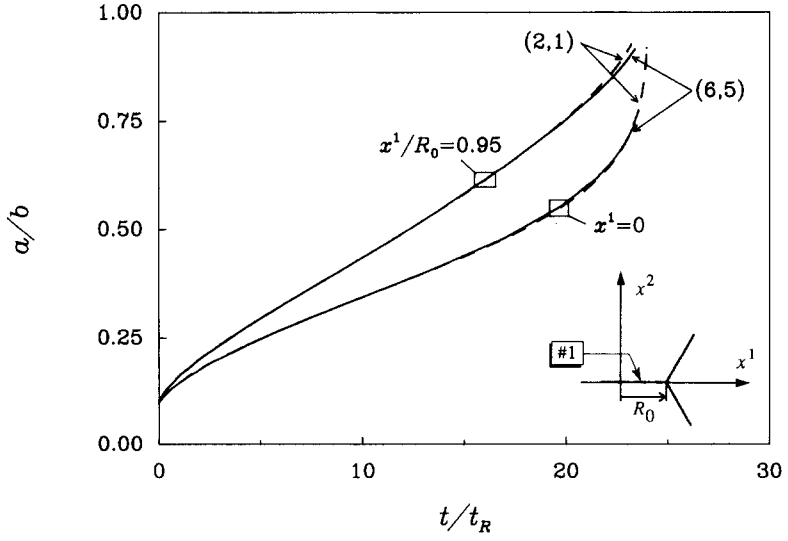

Fig. 9. Development of damage at the central facet #1 in a (m_1, m_2) unit cell with free grain boundary sliding for $\Sigma_1 = 0.5\Sigma_2$, $(a/L)_I = 0.1$ and $F_n = 0$, with $a_I/R_0 = 0.01$ and $b_I/R_0 = 0.1$.

material parameters (see Fig. 8). For all cells, the effect of suppressing sliding is to increase the time to coalescence by a factor of about 6, just like in the axisymmetric cell model study of Van der Giessen and Tvergaard (1991a). A comparison of Fig. 8 and Fig. 7 shows that the position of

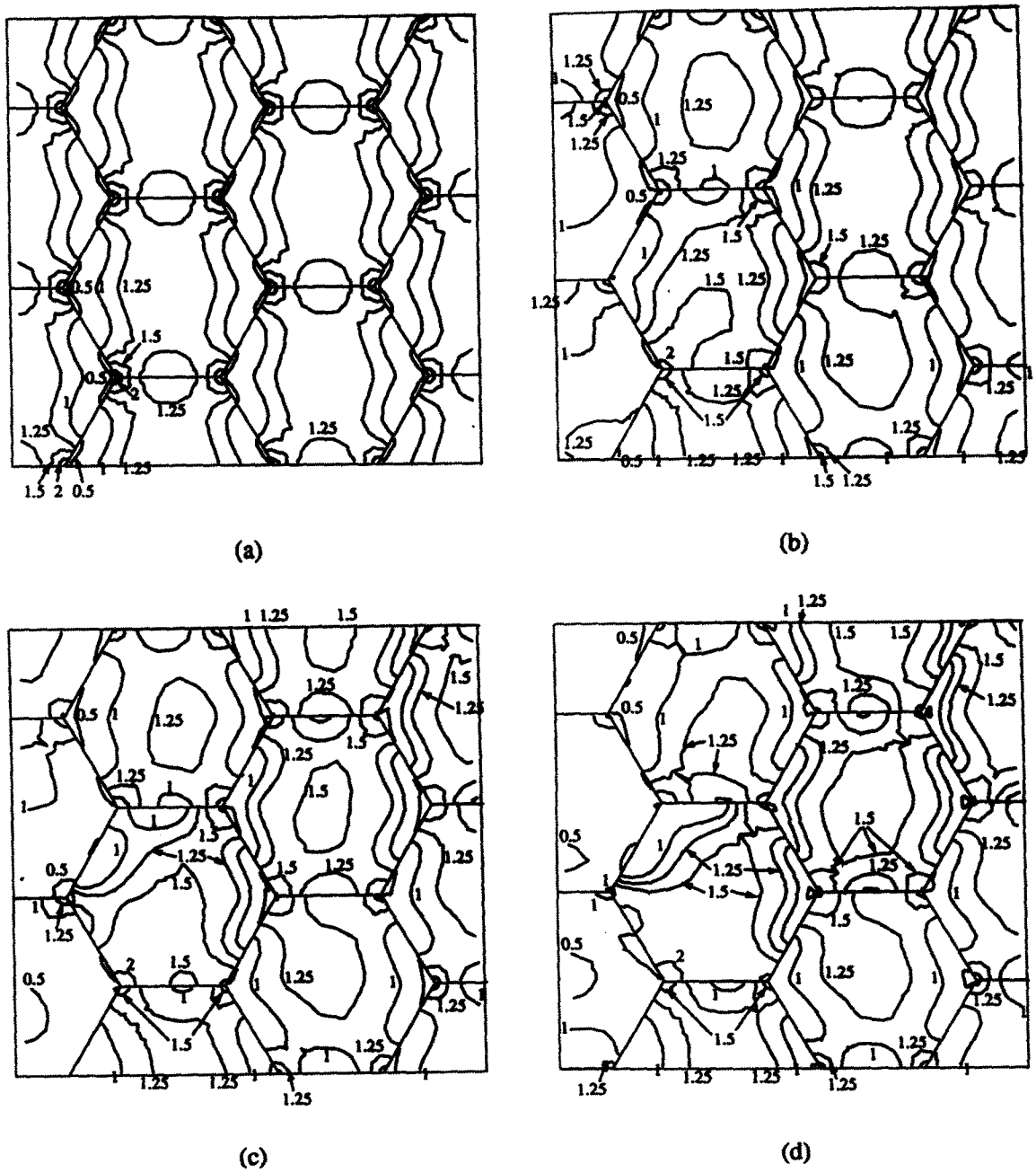

Fig. 10. Contours of the normalized Mises stress σ_e/Σ_e in the (6, 5) unit cell for the case shown in Fig. 7 at: (a) $t/t_R = 0$; (b) $t/t_R = 0.25$; (c) $t/t_R = 0.5$; (d) $t/t_R = 1$.

the various cavity growth results relative to each other are not significantly influenced by grain boundary sliding, but for a given cell size the interaction appears to be somewhat stronger in the case of free sliding (for instance, the results for the (4, 2) and (6, 3) cell are relatively closer in Fig. 8). In the sequel we shall concentrate only on polycrystals with free sliding.

Some of the cases shown in Fig. 7 have been repeated for a lower value of the diffusion parameter $\mathscr{D}$, specified by $(a/L)_I = 0.1$. Only the two extreme cells are considered in Fig. 9, namely the (2, 1) unit cell where the cavitating facets are very closely spaced and the (6, 5) cell which represents a case with well-separated facets. As opposed to Fig. 7, cavitation on the central facet is rather non-uniform in the cases of Fig. 9; therefore, cavity growth results are presented both at the center of the facet and near the triple point. An even more important difference from Fig. 7 is that the results for the two cells in Fig. 9 are virtually identical, although the facet density differs by a factor of 15. The difference between Figs. 7 and 9 can be understood by noting that for the cases in Fig. 7, where $(a/L)_I = 0.025$, the diffusion rate is quite high relative to the creep rate, so that cavity growth is strongly constrained by the creep deformations of the surrounding grains, whereas this creep constraint is not active when $(a/L)_I = 0.1$ as used in Fig. 9. As has been noted by several authors (e.g., Argon 1982; Tvergaard, 1984, 1985), creep constrained cavity growth is characterized by severe stress redistributions inside the polycrystalline aggregate resulting from the need to accommodate the thickening rate $\dot{\delta}_c$ of the grain boundary layer due to cavitation by the creep deformations of the grains. After a certain transient period, this gives rise to very much reduced normal stresses on the cavitating grain boundary facets relative to the macroscopic resolved normal stress, such that the creep deformations of the grains themselves become comparable to those discussed previously when the grain boundary facet has been completely cracked. This stress redistribution causes the strong sensitivity to the density of cavitating facets found in Figs. 7 and 8. On the other hand, in the absence of creep constraint (Fig. 9) there is no stress redistribution and therefore no sensitivity to either cell size or cell aspect ratio.

As an illustration of the stress redistributions associated with creep constrained cavitation, Fig. 10 shows the distribution of the local Mises effective stress inside the (6, 5) cell at four different

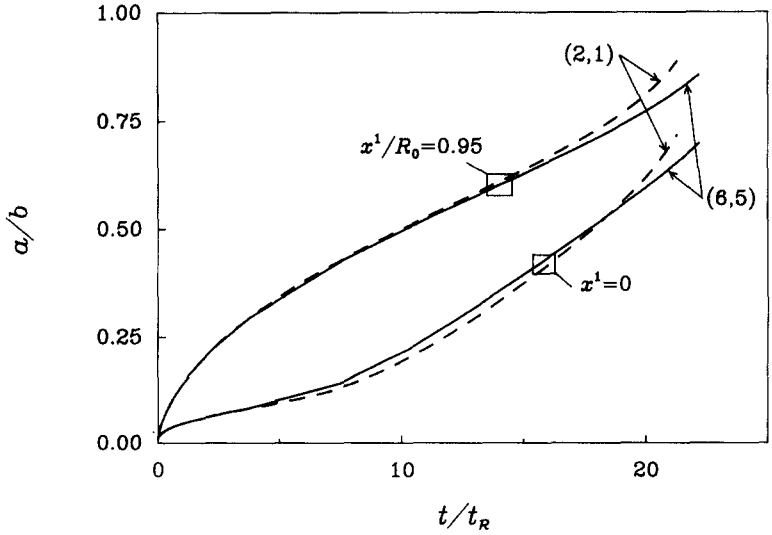

Fig. 11. Development of damage at the central facet #1 in a (m_1, m_2) unit cell with free grain boundary sliding for $\Sigma_1 = 0.5\Sigma_2$, $(a/L)_I = 0.025$ and $F_n = 100N_I$, with $a_I/R_0 = 0.01$ and $b_I/R_0 = 1$.

instants during the rupture life time. The particular case shown corresponds to the parameters used in Fig. 7. Figure 10a shows the initial elastic stress distribution in a polycrystal with free sliding. In Fig. 10b, corresponding to $t/t_R = 0.25$, it is seen first of all that local creep deformations have reduced the grain boundary sliding induced stress concentrations at the triple points. Furthermore, it is observed that already at this level of cavitation ($a/b = 0.43$ at the center) a significant change in the stress distribution has occurred, with released stresses inside the central grain containing the cavitating facet and load shedding to the neighbouring grains. This load shedding process is seen to continue in Figs. 10c and 10d. In the last contour plot, corresponding to $t/t_R = 1$ and a high level of cavitation ($a/b = 0.75$ at the center), the highest overall levels of the Mises stress appear in the band of grains running from the central one to the top right-hand corner of the quarter cell. Thus, the creep deformations needed to accommodate the cavitation tend to be somewhat concentrated in this band of grains.

In the foregoing analyses, all cavities were assumed to be present from the beginning of the process. This represents situations where cavity nucleation saturates early in the creep rupture process. Now, Fig. 11 shows some results when continuous cavity nucleation takes place starting from an initially low cavity density N_I as specified by the initial spacing $b_I/R_0 = 1$. Just like in previous studies (e.g., Van der Giessen and Tvergaard, 1990, 1991b,c) a value of $F_n = 100N_I$ is used in the nucleation law (7), while the parameter Σ_0 is chosen to be equal to the macroscopic effective stress Σ_e. The applied stress state and remaining material parameters are taken as in Fig. 7. Results are shown in Fig. 11 only for the (2, 1) and (6, 5) cell, respectively, and it is seen that there is much less interaction now between cavitating facets than in the corresponding cases without nucleation shown in Fig. 7. It is only at the last stages of the process that the interaction becomes noticeable in the acceleration of the growth of a/b in the (2, 1) unit cell. This is to be attributed to the fact that for this value of the parameter F_n, nucleation is so slow that the cavitation process is largely nucleation controlled, as

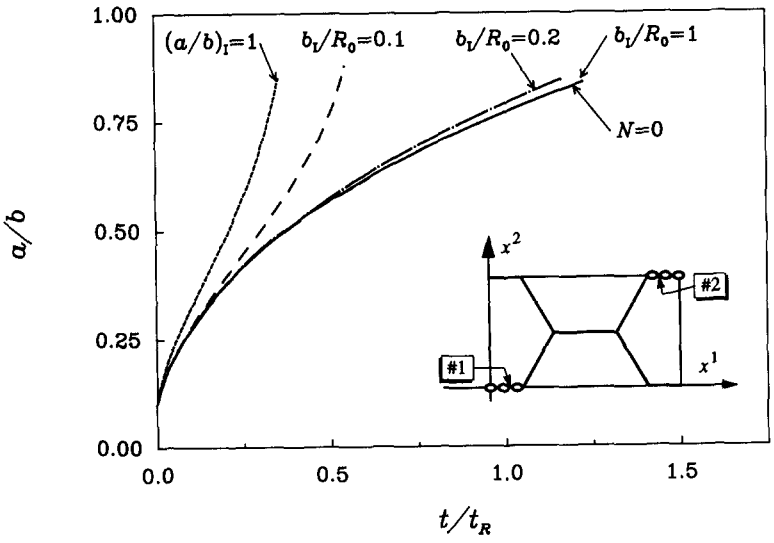

Fig. 12. Development of damage at the center of the central facet #1 in a (4, 2) unit cell with two differently cavitating facets and free sliding for $\Sigma_1 = 0.5\Sigma_2$. Cavitation on both facets is characterized by $(a/L)_I = 0.025$, $a_I/R_0 = 0.01$, $F_n = 0$. The cavity density on the central facet is taken according to $b_I/R_0 = 0.1$, while different initial cavitation conditions are considered on the #2 facet, as indicated.

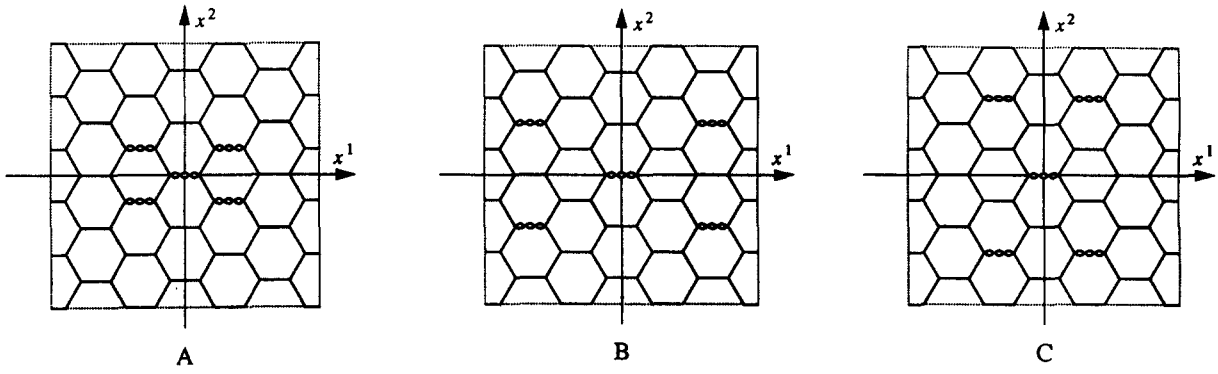

Fig. 13. Different morphologies of a (6, 5) unit cell containing two families of cavitating facets.

noted before by Van der Giessen and Tvergaard (1990), so that creep constrained cavitation does not occur before the final stages.

4.3. *Clustering of cavitating facets*

In the previous subsection, the cavitating facets were assumed to be homogeneously distributed throughout the polycrystal, so that they all behaved identically. Here we will study the effect of clustering of cavitating facets by considering cavitation to occur on the #1 facets as well as on the #2 facets (see Fig. 2). The interaction is expected to depend on the relative position of the cavitating facets, and also on the different nucleation rates or different initial cavitation states on the two groups of facets.

In Fig. 12 we consider a (4, 2) cell with the #2 facet located as indicated in the insert. The material parameters are taken to be the same as in Fig. 7, and also the initial cavitation state on the #1 facet is taken to be identical. Various initial cavitation conditions on the #2 facets are considered, ranging from no cavitation at all ($N = 0$),

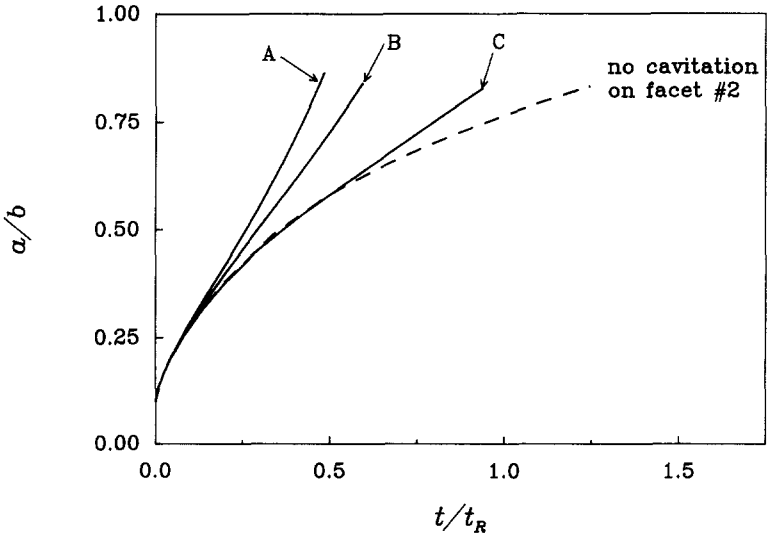

Fig. 14. Developments of damage at the center of the central facet #1 in a (6, 5) cell for various distributions of the #2 facets. The results are for $\dot{\epsilon}_e^C/\dot{\epsilon}_B = 0$, $\Sigma_1 = 0.5\Sigma_2$, and with $(a/L)_I = 0.025$, $a_I/R_0 = 0.01$, $b_I/R_0 = 0.1$, $F_n = 0$ on facets #1 as well as #2.

via an identical cavity spacing on the two groups of facets ($b_1/R_0 = 0.1$), to a full facet microcrack from the beginning ($(a/b)_I = 1$); no nucleation is assumed in these analyses. Figure 12 shows that the cavity growth at the center of the central facet #1 is not affected by simultaneous growth on the secondary facets as long as the number of cavities present there is less than, say 25% of those on the central facet. When there is an identical or larger number of cavities on the facets #2 a strong interaction between the two facets becomes apparent, even though the facets are not immediate neighbours. For the stress state and material properties considered here,

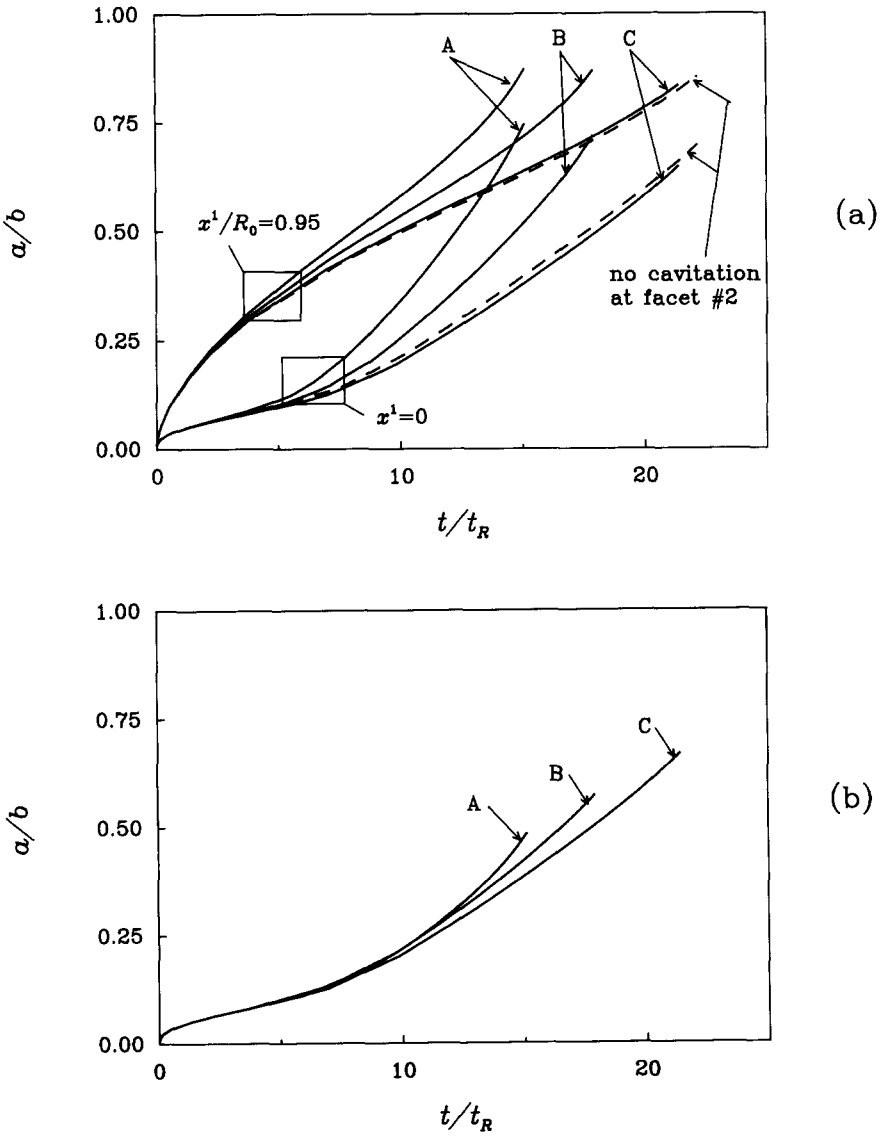

Fig. 15. Development of damage in a (6, 5) cell for various distributions of the #2 facets. The results are for $a_I/R_0 = 0.01$, $b_I/R_0 = 1$, $F_n = 100N_I$ on facets #1 as well as #2, with $\dot{\epsilon}_e^C/\dot{\epsilon}_B = 0$, $\Sigma_1 = 0.5\Sigma_2$, $(a/L)_I = 0.025$ just as in Fig. 14: (a) at two positions on the central facet; (b) at the center of facet #2.

this interaction can reduce the time to coalescence by a factor of 4; but, it should be recalled that the value $(a/L)_I = 0.025$ used here implies a significant creep constraint on cavitation. For larger values of $(a/L)_I$ this interaction will diminish.

We now proceed by studying the effect of different morphologies of the distribution of cavitating facets. Figure 13 shows three different distributions, A thru C, of the #2 facets around the central #1 facet in a (6, 5) unit cell. The density of cavitating facets in all three morphologies is $\rho = 0.016$. Figure 14 shows results for cavity growth on the central facet #1 for the same conditions and material parameters as in Fig. 7, but assuming an identical cavity density and initial cavity size on both families of facets. Cavitation on the secondary facets is seen to increase the rate of creep in the material around the central facet, thus leading to enhanced cavity growth. But, the effect strongly depends on clustering. The largest enhancement is observed for morphology A; in that case, cavity growth is found to be faster than for the smallest cell considered in Fig. 7 with a three times higher density ρ, and about as fast as the growth for $b_I/R_0 = 0.1$ in Fig. 12. What is particularly interesting to note is the remarkable difference between the results for the B and C morphologies, even though the distance between the #1 and #2 facets differ rather little. This shows that the interaction between cavitating facets depends on their mutual geometric location, and that the average distance does not correlate well with the strength of the interaction for the material parameters considered here.

The analyses have been repeated taking into account nucleation of new cavities as specified by $F_n = 100N_I$, $b_I/R_0 = 1$ on both families of facets, and otherwise identical parameters as in Fig. 14. The results in Fig. 15a show a significant effect of the morphology of the distribution of cavitating facets. This is somewhat surprising, since in Fig. 11 we found that cavitation in such cases with a rather low nucleation rate is only slightly affected by the density of cavitating facets. As shown in Fig. 15b, cavity nucleation and growth at the center of the #2 facets have been comparable to that on the central facet; but the effect of the three morphologies seems to be smaller.

In the cases considered in Fig. 15, the nucleation rate parameter F_n was taken to be the same on the two families of facets. We have repeated the analysis for morphology A with other values

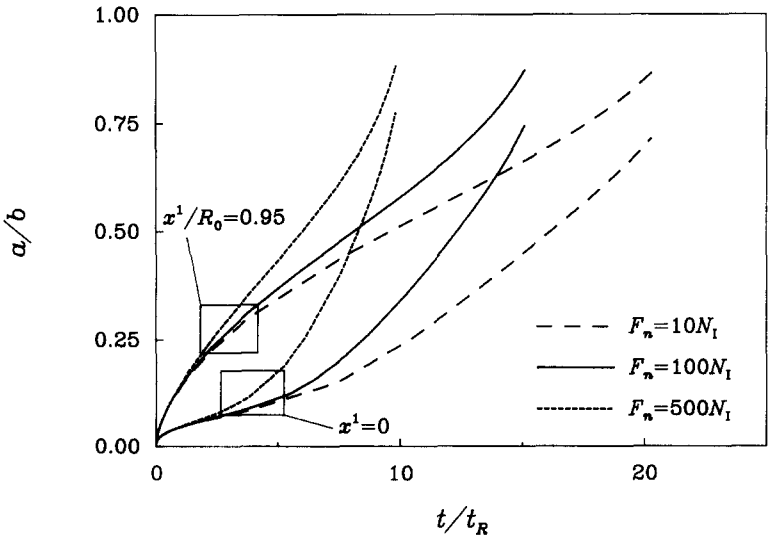

Fig. 16. Development of damage at the central facet in a (6, 5) cell for $\dot{\epsilon}_e^C/\dot{\epsilon}_B = 0$, $\Sigma_1 = 0.5\Sigma_2$, $(a/L)_I = 0.025$, $a_I/R_0 = 0.01$, $b_I/R_0 = 1$, and with $F_n = 100N_I$ on the central facet. The values of F_n on the #2 facets are as indicated.

of on the #2 facets, while keeping all other parameters as in Fig. 15. A ten times lower value of F_n on the #2 facets is seen in Fig. 16 to put a somewhat higher constraint on the development of damage on the central facet, thus increasing the time to coalescence by around 30%. Similarly, the time to coalescence is reduced by around 30% when F_n is five times larger on the #2 facets than on the central facet. The variations of F_n considered here, however, are probably relatively large; variations within a factor of 2 will only have a minor effect on cavitation in these cases.

5. Discussion

The present numerical study for a rather large planar unit cell containing many grains allows for a detailed investigation of the effect of distribution as well as density of cavitating grain boundary facets. Most previous investigations have been based on analyses for unit cell models containing only a single grain or a few grains, and only the model of Hsia et al. (1991) for an open microcrack has incorporated the complexity of many grains sliding freely against one another, while each grain deforms elastically and by power law creep. In the present paper the many grain model has been extended to account for the possibility of cavity nucleation and growth on all grain boundary facets, and also the effect of grain boundary viscosity has been incorporated following the methods used in previous studies by the authors (Van der Giessen and Tvergaard, 1991a, 1991c). For an open microcrack at a grain boundary facet surrounded by freely sliding grains the results in Table 1 appear to be in good agreement with those of Hsia et al. (1991). The computed crack opening rates are here related to the expression (17) or (14) of the form first suggested by Rice (1981), because this expression has the advantage over the curve fitted expression of Hsia et al. (1991) that the possibility of nonzero normal stresses on the crack surfaces is accounted for, so that (17) or (14) are well suited to also model effects on grain boundary cavitation (see Tvergaard, 1985). Table 1 shows that for a given value of the crack density the crack opening rate depends strongly on the cell aspect ratio, which represents the ratio of the crack spacings in the axial and transverse directions. For a given aspect ratio the results show that in an aggregate of freely sliding grains the effect of crack density is well represented by using a function $c_2(\rho)$ in (17) and (18), which increases for increasing value of ρ, and the same tendency is indicated by a few results for axisymmetric or full 3D cell model studies (see Table 3). In fact, the crack opening rate and thus the value of c_2 grows very large when the crack density reaches a limiting value of $\rho = 0.096$ in plane strain, or $\rho \approx 0.04$ in the full 3D case. Furthermore, for a given crack density the value of c_2 is a strongly increasing function of the creep exponent n (see Table 1).

When cavity growth takes place on the central facet of the unit cell, the predicted cavity growth rates reflect the crack opening rates found in Table 1, as long as diffusive cavity growth is rapid enough to give creep constrained cavitation. Both for free grain boundary sliding (Fig. 7) and for practically no sliding (Fig. 8) the cavity growth rate increases monotonically with increasing density of cavitating facets, as long as the aspect ratio of the unit cell does not change. As expected based on the results for an open microcrack, the cavity growth rate is quite sensitive to the aspect ratio of the unit cell, and the sensitivity to both aspect ratio and cavitating facet density is much more dramatic with free grain boundary sliding than with no sliding. The behaviour is rather different in cases where diffusive cavity growth is less rapid, so that creep constrained cavitation does not develop (Fig. 9). With no creep constraint no stress redistribution occurs, and then the cavitation behaviour is rather insensitive to the density of cavitating facets and to the unit cell aspect ratio. Similar behaviour is found when the lack of creep constraint on cavitation results from rather slow continuous cavity nucleation, as in Fig. 11.

It has been found that under creep constrained cavitation conditions, cavity growth is very sensitive to the spacing between cavitating facets in the transverse direction, as characterized by the value of m_1/m_2. In this connection, it is noted that unit cell models for freely sliding

polycrystals with $m_2 = 1$ are tantamount (but not equivalent) to Chokshi's (1987) one-dimensional two-bar model. He concluded from such a model that during constrained cavity growth the interaction between cavitating facets is significant up to transverse spacings corresponding to $m_1 = 10$ in our terminology, while the cavity growth rates decrease substantially with increasing transverse spacing. Although we have not actually carried out an analysis for this m_1 value, the results in Fig. 7 seem to support this qualitatively. However, aspect ratios of $m_1/m_2 \approx 10$ are not realistic and one would rather expect aspect ratios around 1. The cell with $(m_1, m_2) = (6, 5)$ analyzed here is probably more realistic, and it has been found that in that case interaction between cavitating facets has virtually disappeared.

The rather large unit cell containing many grains is well suited for studies of nonuniformly distributed cavitating facets. Clustering of cavitating facets is found to strongly affect the rate of cavity growth in cases where creep constrained cavitation develops. Thus, for the same density of cavitating facets some distributions give strongly increased cavity growth rates due to the interaction between neighbouring cavitating facets, whereas other distributions give rather little interaction (see Figs. 13 and 14). This is partly explained by the redistribution of effective Mises stresses shown in Fig. 10 for an aggregate of freely sliding grains around a facet where creep constrained cavitation develops. After full stress redistribution the highest levels of Mises stress appear in a band of grains at an angle of about 45 degrees from the cavitating facet, and it seems obvious that the effect of a neighbouring cavitating facet would be stronger the higher the stress level is in this redistributed stress field. Also the effect of continuous cavity nucleation on interacting facets in a cluster has been analysed, and it has been found that cavitation may be strongly delayed, if nucleation occurs much more slowly on one of the interacting facets.

It is emphasized that the kind of interaction studied in this work acts on the size scale of several grains. The creep rupture process involves also interaction on a smaller size scale, namely between growing cavities on a single grain boundary facet. No attempt is made here to model this type of interaction, just like in previous studies by Needleman and Rice (1980), Argon (1982), Cocks and Ashby (1982), Tvergaard (1984). This is partly justified by the fact that when the distribution of cavities over a facet is smooth, the cavity spacing is large enough during the largest part of the life time to exclude interaction between them. Nevertheless, when clustering of cavities occurs, this type of interaction may become significant, and this has been studied in some detail by Wilkinson (1988). He concluded that the stress and temperature dependence of cavity growth is not appreciably affected by clustering, but that the actual average cavity growth for heavily clustered distributions can be reduced considerably due to accomodation requirements. As a consequence, the cavity growth rates computed from our model will give a conservative estimate of the time to coalescence in such extreme cases.

In the present paper, the planar multi-grain cell model has been used to study the effect of neighbouring cavitating facets on the cavity growth rate, and the effect of cavitating facet density on this growth rate. The multi-grain cell model also allows for the possibility of continuing the computations until microcracks start to develop by cavity coalescence on facets, and the model is able to describe the subsequent coalescence of neighbouring microcracks by grain boundary sliding or cavity coalescence on intermediate facets, thus leading to the gradual formation of a macroscopic crack. Such rather elaborate computations based on the present model are carried out currently by the authors and will be reported elsewhere.

Acknowledgement

The work of EvdG was made possible by a fellowship of the Royal Netherlands Academy of Arts and Sciences.

References

Anderson, P.M. and J.R. Rice (1985), Constrained creep cavitation of grain boundary facets, *Acta Metall. 33*, 409–422.

Argon, A.S. (1982), Mechanisms and mechanics of fracture in creeping alloys, in: B. Wilshire and D.R.J. Owen, eds., *Recent Advances in Creep and Fracture of Engineering Materials and Structures*, Pineridge Press, Swansea, pp. 1–52.

Ashby, M.F. (1972), Boundary defects and atomistic aspects of boundary sliding and diffusional creep, *Surface Sci. 31*, 498–542.

Ashby, M.F. and B.F. Dyson (1984), Creep damage mechanics and micromechanisms, Nat. Physics Laboratory Report DMA(A) 77.

Chen, I-W. and A.S. Argon (1981), Creep cavitation in 304 stainless steel, *Acta Metall. 29*, 1321–1333.

Chokshi, A.H. (1987), Analysis of constrained cavity growth during high temperature creep deformation, *Mater. Sci. Technol. 3*, 656–664.

Cocks, A.C.F. and M.F. Ashby (1982), On creep fracture by void growth, *Progr. Mater. Sci. 27*, 189–244.

Crossman, F.W. and M.F. Ashby (1975), The non-uniform flow of polycrystals by grain-boundary sliding accomodated by power-law creep, *Acta Metall. 23*, 425–440.

Dyson, B.F. and M.S. Loveday (1980), Low ductility creep fractures in 316 stainless steel, in: *Engineering Aspects of Creep*, Inst. of Mechanical Engineers, London, pp. 61–66.

Dyson, B.F. (1983), Continuous cavity nucleation and creep fracture, *Scr. Metall. 17*, 31–37.

Ghahremani, F. (1980), Effect of grain boundary sliding on steady creep of polycrystals, *Int. J. Solids Struct. 16*, 847–862.

He, M.Y. and J.W. Hutchinson (1981), The penny-shaped crack and the plane strain crack in an infinite body of power-law material, *J. Appl. Mech. 48*, 830–840.

Hsia, K.J., D.M. Parks and A.S. Argon (1991), Effects of grain boundary sliding on creep-constrained boundary cavitation and creep deformation, *Mech. Mater. 11*, 43–62.

Needleman, A. and J.R. Rice (1980), Plastic creep flow effects in the diffusive cavitation of grain boundaries, *Acta Metall. 28*, 1315–1332.

Hull, D. and D.E. Rimmer (1959), The growth of grain-boundary voids under stress, *Philos. Mag. 4*, 673–687.

Hutchinson, J.W. (1983), Constitutive behavior and crack tip fields for materials undergoing creep-constrained grain boundary cavitation, *Acta Metall. 31*, 1079–1088.

Needleman, A. and V. Tvergaard (1984), Finite element analysis of localization in plasticity, in: J.T. Oden and G.F. Carey, eds., *Finite Elements, Special Problems in Solid Mechanics*, Vol. V, Prentice-Hall, pp. 94–157.

Pierce, D., C.F. Shih and A. Needleman (1984), A tangent modulus method for rate dependent solids, *Comput. Struct. 18*, 875–887.

Raj, R. and M.F. Ashby (1971), On grain boundary sliding and diffusional creep, *Metall. Trans. 2*, 1113–1127.

Rice, J.R. (1981), Constraints on the diffusive cavitation of isolated grain boundary facets in creeping polycrystals, *Acta Metall. 29*, 675–681.

Riedel, H. (1985), Creep crack growth, in: R. Raj, ed., *Flow and Fracture at Elevated Temperatures*, ASM, Metals Park, Ohio, pp. 149–177.

Saxena, A. and J.L. Bassani (1984), Time-dependent fatigue crack growth at elevated temperature, in: J.M. Wells and J.D. Landes, eds., *Fracture: Interactions of Microstructure, Mechanisms, Mechanics*, The Metallurgical Society of AIME, pp. 357–383.

Sham, T.-L. and A. Needleman (1983), Effects of triaxial stressing on creep cavitation of grain boundaries, *Acta Metall. 31*, 919–926.

Tvergaard, V. (1984), On the creep constrained diffusive cavitation of grain boundary facets, *J. Mech. Phys. Solids 32*, 373–393.

Tvergaard, V. (1985), Effect of grain boundary sliding on creep constrained diffusive cavitation. *J. Mech. Phys. Solids 33*, 447–469.

Tvergaard, V. (1988), Mechanical models of the effect of grain boundary sliding on creep and creep rupture, *Revue Phys. Appl. 23*, 595–604.

Van der Giessen, E. and V. Tvergaard (1990), On cavity nucleation effects at sliding grain boundaries in creeping polycrystals, in: B. Wilshire and R.W. Evans, eds., *Creep and Fracture of Engineering Materials and Structures*, Elsevier, Swansea, pp. 169–178.

Van der Giessen, E. and V. Tvergaard (1991a), A creep rupture model accounting for cavitation at sliding grain boundaries, *Int. J. Fract. 48*, 153–178.

Van der Giessen, E. and V. Tvergaard (1991b), On micro-cracking due to cavitation and grain boundary sliding in creeping polycrystals, in: M. Zyczkowski, ed., *Creep in Structures*, Springer Verlag, Berlin, pp. 295–302.

Van der Giessen, E. and V. Tvergaard (1991c), On the linking-up of microcracks in creeping polycrystals with grain boundary cavitation and sliding, in: A.C.F. Cocks and A.R.S. Ponter, eds., *Mechanics of Creep Brittle Materials–2*, Elsevier, London/New York, pp. 134–145.

Wilkinson, D.S. (1988), The effect of a nonuniform void distribution on grain boundary void growth during creep, *Acta Metall. 36*, 2055–2063.